

Tolerance of the Rieske-type [2Fe-2S] cluster in recombinant ferredoxin BphA3 from *Pseudomonas* sp. KKS102 to histidine ligand mutations

Shigenobu KIMURA^{*1}, Akihiro KIKUCHI[†], Toshiya SENDA[‡], Yoshitsugu SHIRO[†] and Masao FUKUDA[§]

^{*}Graduate School of Life Science, University of Hyogo, Kamigori, Hyogo 678-1297, Japan, [†]Biometal Science Laboratory, RIKEN, Harima Institute/Spring-8, Mikazuki, Hyogo 679-5148, Japan, [‡]Biological Information Research Center (BIRC), National Institute of Advanced Industrial Science and Technology (AIST), Tokyo 135-0064, Japan, and [§]Department of BioEngineering, Nagaoka University of Technology, Nagaoka, Niigata 940-2188, Japan

BphA3 from *Pseudomonas* sp. KKS102 is a Rieske-type [2Fe-2S] ferredoxin that transfers electrons from an NADH-dependent oxidoreductase, BphA4, to a biphenyl dioxygenase complex. A high-level expression and purification system for the recombinant BphA3 in *Escherichia coli* was constructed. Two histidine ligands of the Rieske-type cluster in BphA3, were each replaced with serine, cysteine, asparagine and tyrosine. The single mutants, in which either His⁴⁴ or His⁶⁵ was replaced with a cysteine residue (CH and HC mutants respectively), and the double mutant, in which both histidine residues were replaced with cysteine residue (CC mutant), accumulated to high levels in the *E. coli* cells, while the other single mutants did not. The purified WT (wild-type) protein showed characteristic near-UV and visible absorption and CD spectra of Rieske-type clusters. The X-ray absorption spectra were suggestive of the existence of [2Fe-2S] clusters, with one

histidine and three cysteine ligands in the CH and HC mutants, and an [2Fe-2S] cluster with four cysteine ligands in the CC mutant. The BphA4-dependent cytochrome *c* reductase activities of the mutants were less than 0.3 % of that of the WT protein. The redox potential of the WT protein determined by cyclic voltammetry was -180 ± 5 mV compared with the standard hydrogen electrode, and that of the CH mutant was approx. 175 mV lower. The changes in the near-UV and visible absorption spectra of the mutants showed that the reduced iron–sulphur clusters in the mutants were unstable. His⁴⁴ and His⁶⁵ in BphA3 can be replaced with cysteine residues, but are required for the stabilization of the reduced form of the cluster.

Key words: electron transfer, ferredoxin, histidine ligand, mutation, Rieske-type [2Fe-2S] cluster.

INTRODUCTION

Aromatic compounds are degraded by various aerobic bacteria. *Pseudomonas* sp. strain KKS102 degrades polychlorinated biphenyls, which are known to cause serious problems as environmental pollutants [1]. The degradation of biphenyl compounds by this bacterium begins with dihydroxylation of the aromatic ring by a class IIB multicomponent enzyme system [2] containing a dioxygenase complex (BphA1A2), a ferredoxin (BphA3) and an oxygenase-coupled NADH-dependent ferredoxin reductase (BphA4) [3–5]. BphA4 contains one FAD per molecule, and transfers electrons from NADH to the one-electron carrier BphA3. BphA3 is considered to have one Rieske-type [2Fe-2S] iron–sulphur cluster per molecule, and transfers electrons to BphA1A2. Among these electron-transfer proteins, BphA4 is highly expressed in *Escherichia coli* cells [6]. The tertiary structure of BphA4 was determined by X-ray crystallography, and specific amino acid residues in BphA4, which seem to have a functional significance in electron transfer, were suggested [7]. However, the detailed mechanism of electron transfer between BphA4 and BphA3 is not clear, because high-level expression and purification of recombinant BphA3, which is necessary for crystallization of BphA3 and for biochemical studies on electron transfer, were unsuccessful. Therefore a high-level expression and purification system for recombinant BphA3 is needed.

Ferredoxins are electron-transfer proteins that contain iron–sulphur clusters, such as [2Fe-2S], [3Fe-4S] and [4Fe-4S] [8]. Two

types of [2Fe-2S] clusters are known. One is a plant-type [2Fe-2S] cluster, and the other is a Rieske-type [2Fe-2S] cluster. Both [2Fe-2S] clusters contain two iron atoms, which are bridged by two acid-labile sulphide atoms, but the co-ordination patterns of the amino acid residues around the clusters are different. In plant-type [2Fe-2S] clusters, both of the iron atoms are co-ordinated by the sulphide atoms of two cysteine residues. In Rieske-type [2Fe-2S] clusters, however, one iron atom is co-ordinated by the sulphide atoms of two cysteine residues, and the other iron atom is co-ordinated by the δ -nitrogen atoms in the imidazole rings of two histidine residues (Figure 1) [9–12]. The latter histidine-co-ordinated ferric iron is reduced to a ferrous iron by a one-electron reduction with a higher reduction potential [between +360 and -160 mV compared with the SHE (standard hydrogen electrode)] than that of the plant-type [2Fe-2S] cluster (between -250 and -450 mV compared with the SHE) [13]. It is considered that the difference in the reduction potentials of the plant-type and Rieske-type clusters is mainly due to the amino acid residues that co-ordinate the reducible iron atom, although it was demonstrated that the non-histidine residues, which form hydrogen bonds with Rieske-type [2Fe-2S] clusters in the *Saccharomyces cerevisiae* Rieske iron–sulphur protein [14], in the *Paracoccus denitrificans* cytochrome *bc*₁ complex [15] and in the *Rhodospirillum rubrum* cytochrome *bc*₁ complex [16], also participate in the modulation of the redox properties of the cluster. Kounosu et al. [17] reported that the substitution of His⁴⁶, which is one of the histidine ligands, in the hyperthermostable ARF (archaeal

Abbreviations used: ARF, archaeal Rieske-type ferredoxin from *Sulfolobus solfataricus* strain P-1; BphF, the ferredoxin component encoded by the *bphF* gene from *Burkholderia* sp. strain LB400; Bis, *N,N'*-methylenebisacrylamide; CBB, Coomassie Brilliant Blue; DTT, dithiothreitol; EXAFS, extended X-ray absorption fine structure; FT, Fourier transform; IPTG, isopropyl β -D-thiogalactoside; Psb5R, solubilized domain of porcine liver NADH-cytochrome *b*₅ reductase; RBS, ribosome-binding site; SHE, standard hydrogen electrode; WT, wild-type.

¹ To whom correspondence should be addressed (email s-kimura@sci.u-hyogo.ac.jp).

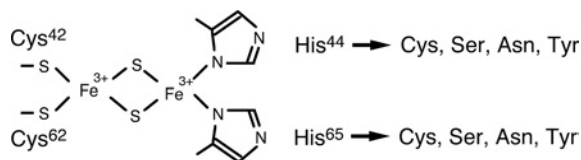


Figure 1 Mutations of His⁴⁴ and His⁶⁵ in BphA3

Predicted structure of the oxidized Rieske-type [2Fe-2S] cluster and ligand residues in BphA3. His⁴⁴ and His⁶⁵ were replaced with cysteine, serine, asparagine and tyrosine residues.

Rieske-type ferredoxin from *Sulfolobus solfataricus* strain P-1) with a cysteine residue lowered the reduction potential by at least 300 mV.

A highly conserved metal-binding amino acid sequence motif, CXHX₁₅₋₂₁CX₂H has been found in all Rieske proteins [2]. This motif contains two cysteine and two histidine residues, which co-ordinate the Rieske-type [2Fe-2S] cluster. BphA3 has this sequence motif, which includes Cys⁴², His⁴⁴, Cys⁶² and His⁶⁵. In the crystal structure of BphF (the ferredoxin component encoded by the *bphF* gene from *Burkholderia* sp. strain LB400), which is a homologue of BphA3 with 71 % amino acid sequence identity with BphA3, the corresponding His⁴⁵ and His⁶⁶ are co-ordinated to the Rieske-type [2Fe-2S] cluster [18,19]. Therefore it is certain that His⁴⁴ and His⁶⁵ in BphA3 are the ligands of the Rieske-type [2Fe-2S] cluster. However, the requirement and role of the histidine ligands of the Rieske-type [2Fe-2S] cluster in BphA3 in electron transfer from BphA4 have not been elucidated.

In the present study, a high-level expression system for the WT (wild-type) *bphA3* gene was constructed in *E. coli* cells, and the recombinant WT BphA3 was purified. Using this expression system, His⁴⁴ and His⁶⁵ in the WT protein were systematically replaced with serine, cysteine, asparagine and tyrosine residues to analyse the tolerance of the protein for these amino acid substitutions. The mutant proteins in which either His⁴⁴ or His⁶⁵ was replaced with a cysteine residue (CH and HC mutants respectively), and that in which both histidine residues were replaced with cysteine residues (CC mutant), accumulated to a high level in *E. coli* cells, and were purified. We describe the spectral properties and BphA4-dependent cytochrome *c* reductase activities of these mutants. We demonstrate that both His⁴⁴ and His⁶⁵ in BphA3 can be replaced by cysteine residues, but these histidine residues are required for the stabilization of the reduced form of the iron-sulphur cluster.

EXPERIMENTAL

Materials

Enzymes for recombinant DNA technology were from TaKaRa (Osaka, Japan). BphA4 from *Pseudomonas* sp. strain KKS102 was expressed in *E. coli* JM109 containing plasmid pKH204 [4], and was purified as described previously [6], except that DE52 (Whatman) was used instead of Q-Sepharose. NADH was from Oriental Yeast Co. (Tokyo, Japan). Cytochrome *c* from bovine heart was from Sigma.

Expression and purification of BphA3

The expression plasmid pCW_{ori}⁺ [20] was used for the synthesis of BphA3 in *E. coli* cells. The DNA encoding BphA3 was amplified by PCR from the plasmid pQE30A3 with the forward primer 5'-TAGGAGGTCATATGACGTTTACCAAAGC-3', which has an NdeI site (underlined) containing the nucleotides encoding the

initiator methionine codon (bold) followed by the nucleotide sequence encoding the N-terminal peptide of BphA3 (Primer-1), and the reverse primer 5'-CCGCCAAGCTTCTATCAGGCATG-CAGCGC-3', which corresponds to the C-terminal tetrapeptide, two stop codons and the underlined HindIII site (Primer-2). The plasmid pQE30A3 carries the SacI/HindIII fragment with the *bphA1A2A3B* gene cluster containing the *bphA3* gene [5]. The resulting fragment was inserted into pCW_{ori}⁺ using NdeI and HindIII sites to construct pCA3, which is the expression plasmid for the WT protein. The entire nucleotide sequence encoding BphA3 in pCA3 was confirmed using an ABI PRISM 310 Genetic Analyzer. *E. coli* BL21 cells containing pCA3 were cultivated in Terrific broth containing 0.1 mg/ml ferric ammonium citrate, 1 mM cysteine and 50 µg/ml ampicillin at 37 °C. When the *D*₆₀₀ was approx. 0.3, IPTG (isopropyl β-D-thiogalactoside) was added to a final concentration of 0.2 mM, and cultivation was continued for 30 h. BphA3 was purified at 4 °C as follows. The cells from 2.1 litres of culture fluid were lysed on ice by sonication in 60 ml of buffer A [25 mM potassium phosphate (pH 7.0) containing 1 mM EDTA, 1 mM DTT (dithiothreitol) and 2 % (w/v) glycerol] containing 2 mM PMSF, with a model 450 sonifier (Branson Ultrasonic). The lysate was subjected to centrifugation at 18000 *g* for 20 min. The supernatant was diluted approx. 4-fold with buffer A, and applied to a DE52 column (1.5 cm × 15 cm) equilibrated with buffer A. After the column was washed with buffer A, the proteins were eluted with buffer A containing 0.5 M NaCl. Brown-coloured fractions containing BphA3 were separated on Sephadex G-100 (Amersham Biosciences) column (5 cm × 45 cm) equilibrated with buffer A, collected and applied to a DE52 column (1.5 cm × 20 cm) equilibrated with buffer A. Absorbed proteins were separated with a linear gradient of NaCl from 0 to 0.3 M in 1 litre of buffer A. The fractions containing BphA3 (82 ml) were diluted 3-fold with buffer A, applied to a short column of DE52 (1.5 cm × 7 cm) and concentrated by elution with buffer A containing 0.5 M NaCl. The concentrated fractions were separated on a Sephacryl S-200 (Amersham Biosciences) column (2.5 cm × 92 cm) equilibrated with buffer A containing 0.15 M NaCl. BphA3, which was eluted as a single peak, was collected, quickly frozen in liquid nitrogen and stored at -80 °C. The purity of the protein was analysed by tricine-SDS/PAGE with a 4 %T, 3 %C stacking gel, a 10 %T, 3 %C spacer gel, and a 16.5 %T, 3 %C separating gel [21]. Where the % T and % C are the percentage (w/v) of the sum of the weight of acrylamide and Bis (*N,N'*-methylenebisacrylamide), and the percentage (w/w) of the weight of Bis in the sum of the weight of acrylamide and Bis respectively. Proteins on the gel were stained with CBB (Coomassie Brilliant Blue) R-250.

Mutagenesis, expression and purification of the mutant BphA3 proteins

Before generating the restricted random mutations of His⁴⁴ and His⁶⁵, an XbaI site was introduced as a silent mutation by changing the nucleotide sequence encoding Tyr⁵⁴-Leu⁵⁵-Asp⁵⁶ (TACC-TCGAC) in the WT *bphA3* gene to TATCTAGAC containing an XbaI site (underlined) in order to conveniently construct the mutant genes, which contain mutations at the nucleotides encoding amino acid residues at positions 44 and 65. The silent mutation was introduced by PCR using Primer-2 containing a HindIII site, the forward primer 5'-CCGGATCCATCGATGCTTAGG-3' (Primer-3), which has the same nucleotide sequence (containing the underlined BamHI site) as that upstream of the NdeI site in pCA3, and the mutagenic forward primer 5'-CGAAGGTGG-CTATCTAGACGGCGATGTCG-3' containing the underlined

XbaI site (Primer-4). At first, a mutant DNA fragment was obtained from pCA3 using Primer-4 and Primer-2. Then, the purified fragment was mixed with pCA3, and re-amplified using Primer-3 and Primer-2. The resulting secondary PCR product was ligated in the plasmid pUC118 using the BamHI and HindIII sites to construct the plasmid pU8A3-*XbaI*.

The mutant genes, in which His⁴⁴ was replaced with cysteine (H44C), serine (H44S), asparagine (H44N) or tyrosine (H44Y) residues, and His⁶⁵ was replaced with cysteine (H65C), serine (H65S), asparagine (H65N) or tyrosine (H65Y) residues, were prepared by restricted random mutagenesis using pU8A3-*XbaI* as the template. The mutagenic forward mixed primers 5'-CAGG-ACCAGTGCACDWRTGGAGAGTGGTCGC-3' (Mixed primers-1) and the reverse mixed primers 5'-CACAAAACCTTC-CCATGYWTAARGAGCATTCCACGAC-3' (Mixed primers-2) were used to generate mutations of His⁴⁴ and His⁶⁵ respectively. In these nucleotide sequences, D is the mixture of A, T and G, W is the mixture of A and T, R is the mixture of A and G, and Y is the mixture of C and T. The DNA fragment mixture encoding His⁴⁴-substituted BphA3s was amplified from pU8A3-*XbaI* with Mixed primers-1 and Primer-2. The purified resulting fragment mixture was mixed with pU8A3-*XbaI*, and re-amplified using Primer-3 and Primer-2. The resulting secondary PCR product mixture was ligated in the plasmid pUC118 using the BamHI and HindIII sites to construct the plasmid mixture pU8A3H44X. *E. coli* JM109 cells were transformed with pU8A3H44X. Plasmids containing the newly introduced PmaCI site (pU8A3H44C), SpeI site (pU8A3H44S) and NdeI site (pU8A3H44Y) were identified from the transformants by restriction site analysis of the plasmids. A clone with the plasmid encoding the H44N mutant (pU8A3H44N) was identified by nucleotide sequencing of the plasmid that did not have these new sites. The DNA fragment mixture encoding His⁶⁵-substituted BphA3 was also prepared from pU8A3-*XbaI* by a similar procedure as the preparation of that encoding the His⁴⁴-substituted BphA3. Primer-3 and Mixed primers-2 were used for the first PCR. The purified resulting fragment mixture was mixed with pU8A3-*XbaI* and re-amplified using Primer-3 and Primer-2. The secondary PCR product mixture was ligated to plasmid pUC118 using the BamHI and HindIII sites to construct the plasmid mixture pU8A3H65X, and *E. coli* JM109 cells were transformed with this plasmid mixture. Clones carrying the plasmid containing the newly introduced EcoT22I site (pU8A3H65C), AflIII site (pU8A3H65S) and DraI site (pU8A3H65N) were identified from the transformants by restriction site analysis of the plasmids. A clone with the plasmid encoding the H65Y mutant (pU8A3H65Y), was identified by nucleotide sequence analysis of the plasmids that did not have these new sites. The mutant *bphA3* gene encoding the mutant protein, in which both His⁴⁴ and His⁶⁵ were replaced with cysteine residues, was constructed by replacing the XbaI/HindIII region in pU8A3H44C with the corresponding XbaI/HindIII region of pU8A3H44C, which resulted in the plasmid pU8A3H44C/H65C. The entire nucleotide sequence of the mutant genes was confirmed by nucleotide sequence analysis.

All of the mutant *bphA3* genes were inserted into pCW_{ori}⁺ using the BamHI and HindIII sites to construct the expression plasmids designated pCA3-XX. The Xs in pCA3-XX are one-letter symbols for cysteine (C), serine (S), asparagine (N) or tyrosine (Y), and the first and second Xs represent one-letter symbols of the amino acid residues at positions 44 and 65 in the mutant BphA3 proteins respectively. For example, the plasmid pCA3-CH is the expression plasmid for the H44C mutant. Mutant proteins were expressed in the soluble fraction of *E. coli* BL21 cells, and were purified using the same method as that used for the WT BphA3 as described above.

Absorption and CD spectra

Absorption and CD spectra were measured at 25 °C in 25 mM potassium phosphate (pH 7.0) containing 2 % (w/v) glycerol, 0.15 M NaCl and 1 mM DTT on a Hitachi U-2010 spectrophotometer equipped with a Lauda RMS thermostatically regulated water bath and on an AVIV 62DS CD spectrophotometer respectively.

X-ray absorption spectroscopy

Iron K-edge X-ray absorption spectra were measured in fluorescence mode with a 19-element Ge solid-state detector (CAN-BERRA) on the bending magnet beam line BL38B1 of the synchrotron radiation facility SPring-8 in Hyogo, Japan (proposal No. R03B38B1-0005N and R03B38B1-0048N). Data collection was under dedicated conditions at 8 GeV and 99–91 mA, using a Si(111) double-crystal monochromator. Harmonic contamination was rejected using a total reflection mirror. The proteins containing approx. 5 mM iron in 25 mM potassium phosphate (pH 7.0), 0.15 M sodium phosphate and 20 % (w/v) glycerol were placed in the sample cells [22], and were flash-frozen in a nitrogen stream at 100 K.

The area of the 1s–3d pre-edge peak was obtained by integrating over a range of 10 eV. Fourier transformations were performed over the *k* range 3–12 Å^{−1} (1 Å = 0.1 nm) using *k*² weighting. The structural parameters were determined by curve-fitting procedures using RIGAKU REX2000 software. Theoretical parameters used in the curve-fitting analysis were calculated by FEFF8.1 [23].

MS and N-terminal amino acid sequence analysis

The molecular mass of protein was measured using a Voyager RP/HK MALDI-TOF (matrix-assisted laser-desorption ionization–time-of-flight) mass spectrometer (PerSeptive Biosystems). The protein was ionized using a matrix solution containing 10 mg/ml 3,5-dimethoxy-4-hydroxycinnamic acid, 0.1 % trifluoroacetic acid and 30 % acetonitrile. Bovine insulin, *E. coli* thioredoxin and horse apomyoglobin (average *m/z* values of [M + H]⁺ are 5734.59, 11674.48 and 16952.56 respectively) were used for the calibration of the peptide mass. The N-terminal amino acid sequence was analysed using a Shimadzu PSQ-1 protein sequencer.

Amino acid analysis and protein assay

The protein concentration of the WT protein solution was determined by amino acid analysis after the hydrolysis of the protein with hydrochloride at 110 °C for 24 and 48 h using a Hitachi L-8500 Amino Acid Analyzer.

Protein assays of purified proteins were performed using the BCA (bicinchoninic acid) protein assay reagent (Pierce), according to the microtitre plate protocol provided by the supplier using BSA as a standard protein.

Detection of acid-labile sulphide and iron concentration

The acid-labile sulphide in the purified proteins was detected by reacting the released sulphide with *N,N'*-dimethyl-*p*-phenylenediamine and ferric chloride under acidic conditions [24]. Iron concentrations were measured using a flameless-type Shimadzu AA-660G atomic absorption spectrophotometer equipped with GFA-4B at 2300 °C for 5 s at 248.3 nm. An iron (III) nitrate standard solution for atomic absorption analysis (Wako Pure Chemical) was used for determining a standard curve.

Cytochrome *c* reduction

BphA4-dependent cytochrome *c* reduction activity of BphA3 was measured in 25 mM potassium phosphate (pH 7.0) containing 2% (w/v) glycerol and 0.15 M NaCl at 25°C. The initial concentrations of cytochrome *c*, BphA4 and NADH in the reaction mixture were 20 μ M, 300 nM and 300 μ M respectively. The reduction rate of cytochrome *c* was measured in the presence and absence of BphA3 using the difference in molar absorption coefficient of cytochrome *c* between the oxidized and reduced states at 550 nm, $2.1 \times 10^4 \text{ M}^{-1} \cdot \text{cm}^{-1}$. The concentrations of BphA4 and NADH were determined using molar absorption coefficients of $1.04 \times 10^4 \text{ M}^{-1} \cdot \text{cm}^{-1}$ at 450 nm and $6.3 \times 10^3 \text{ M}^{-1} \cdot \text{cm}^{-1}$ at 340 nm respectively. The former value was determined by the same method described previously for obtaining the value for Psb5R (the solubilized domain of porcine liver NADH-cytochrome *b*₅ reductase) [25], except that 6 M guanidinium chloride was used instead of sodium *N*-lauroylsarcosine. Since cytochrome *c* was reduced by BphA4 in the absence of BphA3, the BphA4-dependent cytochrome *c* reduction rate of BphA3 was evaluated by subtracting the cytochrome *c* reduction rate in the absence of BphA3 from that in the presence of BphA3. The cytochrome *c* reduction rate constant of BphA3 (*k*) was calculated by dividing the BphA4-dependent cytochrome *c* reduction rate of BphA3 by the iron concentration. The iron concentrations in the reaction mixture including the WT protein, and the CH, HC and CC mutants were 30 nM, 3.0 μ M, 6.0 μ M and 6.0 μ M respectively.

Cyclic voltammetry

The redox potential was analysed by cyclic voltammetry on an ALS Electrochemical Analyzer Model 611B. All measurements were performed in a three-electrode cell with a plastic-formed carbon working electrode (BAS Co.), a platinum wire auxiliary electrode and an Ag/AgCl reference electrode (209 mV compared with the SHE). The redox potentials were converted to the SHE. Proteins were dissolved in 20 mM 3-(*N*-morpholino)propane-sulphonic acid buffer (pH 7.0) containing 80 mM potassium chloride, 1 mM DTT, 2 mM neomycin sulphate and 2% (w/v) glycerol, adopting the experimental conditions for the cyclic voltammetry of BphF [18]. The protein solutions were deoxygenated by bubbling with highly pure argon gas and maintained under an argon gas atmosphere during the measurements. The working electrode was cleaned with a piece of 2000 grid abrasive paper before each measurement.

RESULTS

Expression and purification of the WT BphA3

The WT *bphA3* gene in pCA3 was highly expressed in *E. coli* BL21 cells in the presence of IPTG (Figure 2A). The WT BphA3 was purified from the soluble fraction of the cells by Sephadex G-100, DE52 and Sephacryl S-200 chromatography. At first, 50 mM Tris/HCl buffer (pH 7.5), which did not contain glycerol, was used for the purification of the WT protein (Figure 3B). BphA3 was eluted from the DE52 column as two peaks, which were detected at both 280 and 460 nm (Figure 3B, peaks I and II in a). Peak I was eluted essentially as a single peak following Sephacryl S-200 chromatography (Figure 3B, b). The position of this peak was almost identical with that of chymotrypsinogen A (19.5 kDa). In contrast, peak II separated into two obvious peaks by Sephacryl S-200 chromatography (Figure 3B, c). One was a small peak at the position just after ovalbumin (48.2 kDa), and the other was a larger peak at a position similar to that of Psb5R (30.8 kDa) [25]. These profiles suggest that BphA3 forms

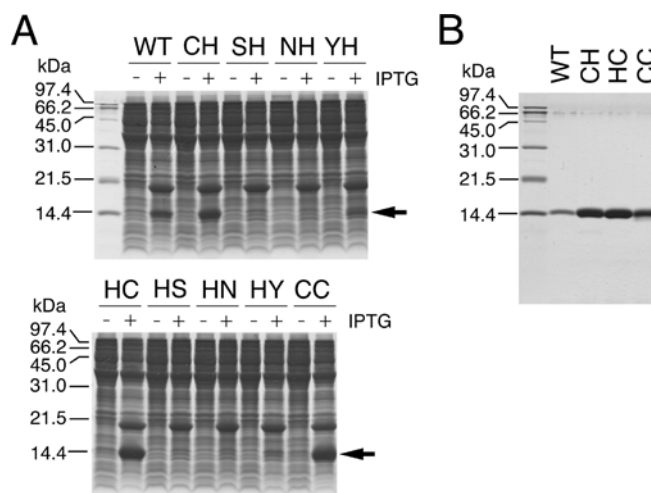


Figure 2 Tricine-SDS/PAGE of whole-cell extracts of *E. coli* cells and purified BphA3s

Proteins on the gel were stained with CBB R-250. (A) Whole-cell extracts from 5 μ l of cultures of *E. coli* BL21/pCA3 (WT), pCA3-CH (CH), -SH (SH), -NH (NH), -YH (YH), -HC (HC), -HS (HS), -HN (HN), -HY (HY) and -CC (CC), which were obtained after cultivation for 30 h in the absence (–) and presence of 0.2 mM IPTG (+), were subjected to electrophoresis, along with SDS/PAGE molecular mass standards (Bio-Rad). Sizes are marked in kDa. The position of the expressed BphA3 is shown with an arrow. (B) Purified fraction of the WT protein (WT), the HC (HC), the CH (CH) and the CC mutants (CC), which contained 200 pmol of iron, were analysed. Molecular mass standards were also electrophoresed, with sizes indicated in kDa.

multimeric forms. However, the WT protein eluted as almost a single peak from the DE52 and Sephacryl S-200 columns using 25 mM potassium phosphate (pH 7.0) containing 2% (w/v) glycerol (Figure 3A). The WT protein was purified with 25 mM potassium phosphate (pH 7.0) containing 2% (w/v) glycerol and 1 mM DTT, as described in the Experimental section. The presence of 1 mM DTT, which was added to prevent intermolecular disulphide bond formation, hardly affected the chromatographic behaviour of the WT protein shown in Figure 3(A).

The purified WT protein showed a single band at a position similar to that of hen's-egg lysozyme (14.4 kDa) after tricine-SDS/PAGE (Figure 2B). The yield of the purified WT BphA3 from 1 litre of culture fluid was 31.6 mg (Table 1). The amino acid sequence Thr-Phe-Thr-Lys-Ala was identified by N-terminal amino acid sequence analysis of the WT protein. The molecular ion peaks measured by MS were at $m/z = 11\,700$ and 5848 . These m/z values were in good agreement with those of the molecular ion peaks of the whole length of the polypeptide portion of the WT from Thr¹ to Ala¹⁰⁸ (molecular mass = 11 696 Da). The amino acid composition of the purified WT protein was consistent with that deduced from the amino acid sequence. These results indicate that the purified WT protein contains a homogeneous polypeptide from Thr¹ to Ala¹⁰⁸.

Spectral properties and iron content of the WT protein

The purified WT protein in the oxidized state showed absorption peaks at 278, 325 and 460 nm, and a shoulder at approx. 580 nm (Figure 4A, a). The spectral shape was characteristic of oxidized Rieske-type [2Fe-2S] iron-sulphur proteins [9,13,18,26]. The CD spectrum of the WT BphA3 showed peaks at 270, 320, 342, 419 and 493 nm, and troughs at 283, 377, 572 and 695 nm (Figure 4B, a). The shape of the CD spectrum of the WT protein at 300–700 nm was almost identical with those of the oxidized Rieske-type iron-sulphur proteins [18,26]. The iron content of the WT protein, which was measured by atomic absorption analysis and

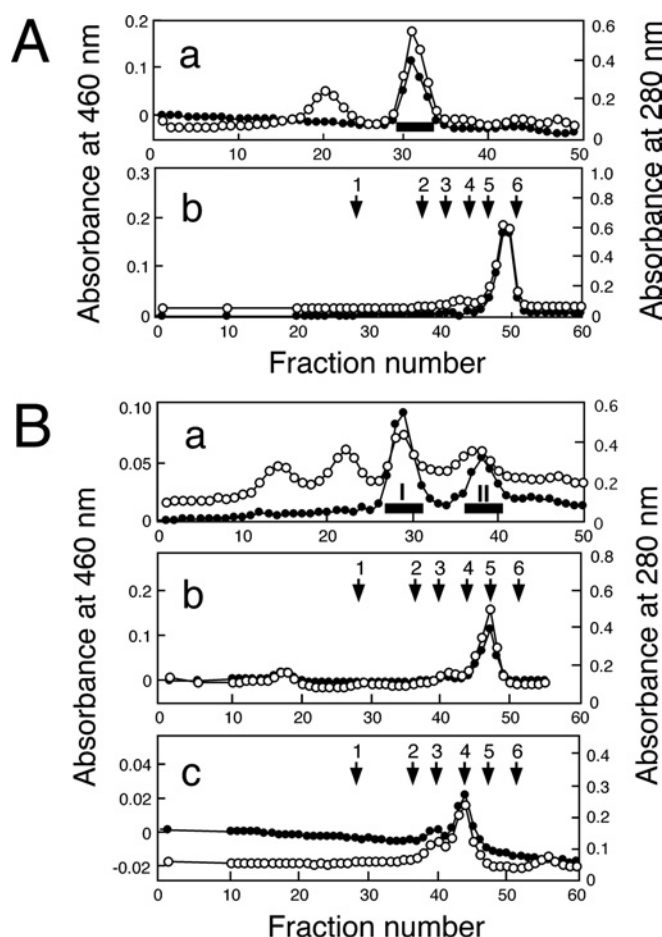


Figure 3 Chromatographic profiles in the purification of the WT protein

The absorbance at 460 nm (●) and 280 nm (○) were plotted against fraction number. **(A)** Elution profiles of the WT protein from the DE52 (a) and Sephacryl S-200 (b) columns in the presence of 2% (w/v) glycerol. The fraction containing the WT protein, which was eluted from the Sephadex G-100 column, was separated using the DE52 column (1.5 cm × 15 cm) equilibrated with 25 mM potassium phosphate (pH 7.0) containing 2% (w/v) glycerol with a linear gradient of NaCl from 0 to 0.25 M (0.5 mM/ml). The volume of each fraction and the flow rate were 16.4 ml and 74 ml/h, respectively. Fractions indicated with a bar were separated using Sephacryl S-200 column (2.5 cm × 92 cm) in 25 mM potassium phosphate (pH 7.0) containing 2% (w/v) glycerol and 0.15 M NaCl. The volume of each fraction and the flow rate were 6.5 ml and 30 ml/h respectively. **(B)** Elution profiles of the WT from the DE52 (a) and Sephacryl S-200 (b and c) columns in the absence of glycerol. In a, the fraction which was eluted from the Sephadex G-100 column was separated using a DE52 column equilibrated with 50 mM Tris/HCl (pH 7.5) with a linear gradient of NaCl from 0 to 0.25 M (0.5 mM/ml). The column size, the volume of each fraction and the flow rate were identical with those in **(A, a)**. Fractions indicated with a bar (peaks I and II) were separated using a Sephacryl S-200 column (b and c respectively) in 50 mM Tris/HCl (pH 7.5). The column size, the volume of each fraction and the flow rate were identical with those in **(A, b)**. In **(A, b)** and **(B, b and c)**, the positions of the peaks of Blue Dextran 2000, albumin (73.5 kDa), ovalbumin (48.2 kDa), Pbs5R (30.8 kDa), chymotrypsinogen A (19.5 kDa) and ribonuclease A (11.9 kDa) are shown with arrows 1–6 respectively.

amino acid analysis, was 1.86 ± 0.09 mol/mol (mean \pm S.E.M.; $n = 5$). Acid-labile sulphide was qualitatively detected with N,N' -dimethyl- p -phenylenediamine and ferric chloride. These results indicate that most of the purified WT BphA3 was holo-protein containing a Rieske-type [2Fe-2S] iron–sulphur cluster.

Expression and purification of the BphA3 mutant proteins

The genes encoding the BphA3 mutant proteins were expressed in *E. coli* BL21 cells (Figure 2A). The whole-cell extracts of BL21/pCA3-CH, -HC and -CC showed that polypeptide chains of the

H44C mutant (CH mutant), the H65C mutant (HC mutant) and the H44C/H65C double mutant (CC mutant) accumulated to a high level like the WT protein. In contrast, the accumulation levels of the polypeptide chains of the H44Y mutant (YH mutant) and the H65Y mutant (HY mutant) were low. The cells that contained the plasmids for the other single mutants showed no obvious band at the position of the WT protein.

The CH, HC and CC mutants were purified with the same method used for the purification of the WT BphA3. All of the mutants were eluted from the Sephacryl S-200 column as essentially a single peak at the same position as the WT protein. The acid-labile sulphide was detected in the purified mutant proteins. The purified mutants showed a single band at the same position as that of the WT protein on the CBB-stained gel after Tricine–SDS/PAGE (Figure 2B). Although the purified protein solutions contained the same amount of iron atoms, the bands of the CH and HC mutants were at least 2-fold, and that of the CC mutant was approx. 1.5-fold, thicker than that of the WT BphA3. The ratios of the protein concentration determined by the protein assay to the iron concentration (protein/Fe values) in the solution of the CH, HC and CC mutants were 2.3-, 2.1- and 1.6-fold that in the solution of the WT protein respectively (Table 1). These results suggest the existence of apo-proteins in the purified mutant protein samples. The contents of the holo-proteins in the purified CH, HC and CC mutant solutions, which were estimated from the protein/Fe values on the assumption that all of the holo-proteins of the mutants contain a [2Fe-2S] cluster, were approx. 45, 50 and 60 % respectively.

Spectral properties of the oxidized BphA3 mutants

All of the purified mutants showed two peaks at 300–700 nm (Figure 4A, b–d). The spectral shape of the HC mutant was very similar to that of the H64C mutant of ARF [17]. The CC mutant showed a sharp peak at 410 nm in addition to the less sharp peaks at 324 and 460 nm. This spectral feature was similar to those of the plant-type [2Fe-2S] ferredoxins [24,27,28]. The apparent molar absorption coefficient (ϵ^{Fe}) values of the CH and HC mutants at 278 nm were 1.8- and 1.6-fold that of the WT protein respectively (Table 1). These values are consistent with the existence of apo-proteins in the purified CH and HC mutant protein samples.

The CD spectra of the purified mutant proteins at 250–800 nm were characteristic of each mutant and different from that of the WT BphA3 (Figure 4B, right). The spectral shape of the HC mutant at 350–700 nm was similar to that of the H64C mutant of ARF [17].

The shapes of the CD spectra of the mutant proteins at 200–250 nm were similar to that of the WT protein (Figure 4B, left). However, the depths of the valleys in the spectra of the CH, HC and CC mutants were approx. 2.5-, 2.5- and 1.3-fold that of the WT protein respectively. These differences in the depths of the valleys are consistent with the presence of apo-proteins in the purified mutant protein samples.

X-ray absorption spectra

The Fe K-edge absorption feature is sensitive to the geometry around the iron atom, and analysis of the 1s–3d pre-edge feature is useful in the determination of the co-ordination number of the iron atom [29]. The normalized 1s–3d pre-edge peak energy of the WT protein, the CH, HC and CC mutants were 0.283, 0.283, 0.276 and 0.275 eV respectively (Figure 5, inset). These values are consistent with the expected values for the four-co-ordinate tetrahedral environment of the iron site. The significant edge-shift and edge-broadening were caused by the replacement of His⁶⁴ in

Table 1 Yields and properties of the purified BphA3s

The yield of purified holo-protein from 1 litre of culture fluid was calculated on the assumption that the holo-protein molecule contains one [2Fe-2S] cluster. The apparent molar absorption coefficient (ϵ^{Fe}) at the peak wavelength (in parentheses) was calculated based on the iron concentration. Protein/Fe is the relative protein concentration, which was determined by the protein assay, to the iron concentration in the purified protein solution. The cytochrome *c* reduction rate constant of BphA3 (*k*) was determined as described in the Experimental section. The values of ϵ^{Fe} , Protein/Fe and *k* are the means \pm S.E.M. of six, three and three measurements respectively.

Protein	Amino acid	Yield (mg)	ϵ^{Fe} ($\times 10^3 \text{ M}^{-1} \cdot \text{cm}^{-1}$)	Acid-labile sulphide	Protein/Fe ($\text{mg} \cdot \mu\text{mol}^{-1}$)	k			
						($\times 10^{-3} \cdot \text{s}^{-1}$)	(%)		
WT	His ⁴⁴	His ⁶⁵ 31.6	10.4 \pm 0.99 (278 nm)	5.96 \pm 0.57 (325 nm)	3.03 \pm 0.29 (460 nm)	Detected	9.4 \pm 0.1	3600 \pm 380	100
CH mutant	Cys ⁴⁴	His ⁶⁵ 9.4	18.2 \pm 1.82 (278 nm)	6.86 \pm 0.69 (327 nm)	3.50 \pm 0.35 (460 nm)	Detected	21.3 \pm 6.3	9.6 \pm 0.95	0.27
HC mutant	His ⁴⁴	Cys ⁶⁵ 14.1	17.1 \pm 1.29 (278 nm)	5.70 \pm 0.43 (328 nm)	3.34 \pm 0.25 (460 nm)	Detected	19.4 \pm 0.2	3.4 \pm 0.17	0.094
CC mutant	Cys ⁴⁴	Cys ⁶⁵ 25.8	10.8 \pm 0.68 (278 nm)	6.42 \pm 0.40 (324 nm)	5.60 \pm 0.35 (410 nm)	Detected	15.3 \pm 0.7	3.5 \pm 0.16	0.097

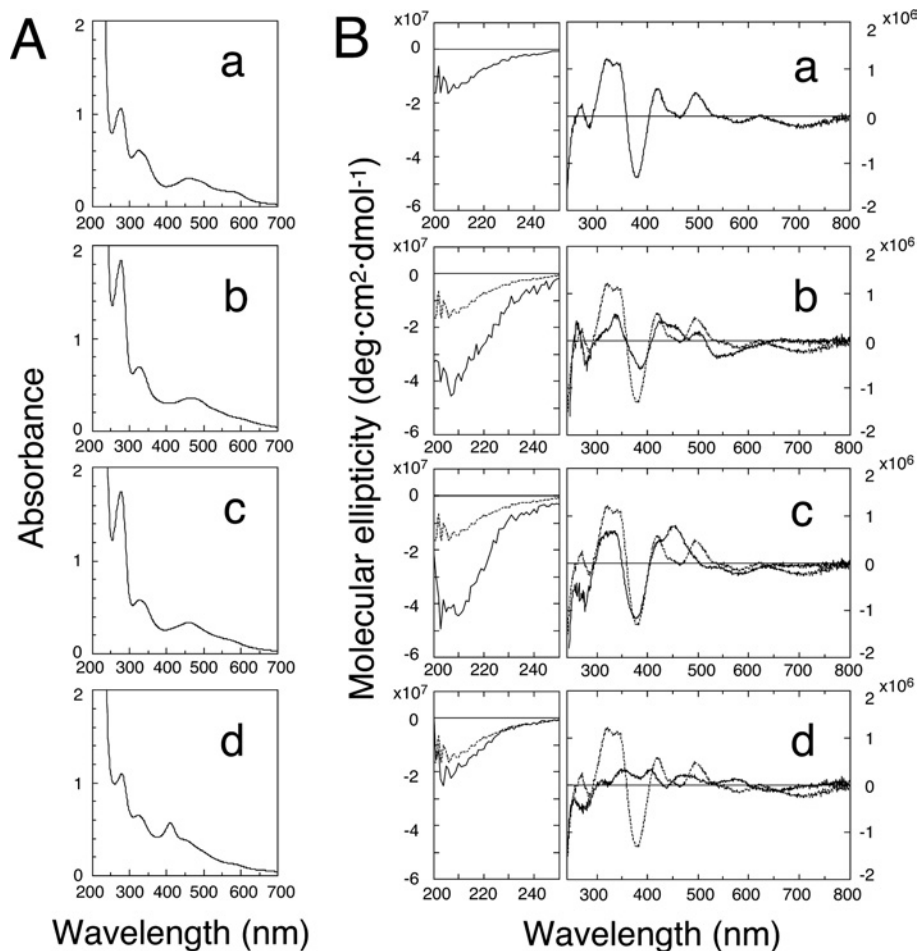


Figure 4 Absorption and CD spectra of oxidized BphA3s

(A) Absorption spectra of the WT protein and the HC, CH and CC mutants containing 100 μM iron (a–d respectively). (B) CD spectra of the WT protein and the HC, CH and CC mutants (a–d respectively). In b–d, the CD-spectrum of the WT protein was superimposed (thin broken line). For the spectra at 200–250 nm, the optical path length was 0.2 mm, and the iron concentrations of the WT protein, and the CH, HC and CC mutants were 471, 88.6, 96.1 and 351 μM respectively. For the spectra at 240–800 nm, the optical path length was 1 cm, and the iron concentrations of the WT protein, and the CH, HC and CC mutants were 102, 88.6, 96.1 and 94.1 μM respectively.

ARF with a cysteine residue [17]. The edge-shifts are explicable as the results of the decrease in the positive charge density on metal atoms by the co-ordination of the more polarized S-donor ligands [30]. However, neither obvious edge-shift nor edge-broadening was observed in the spectra of the BphA3 mutants (Figure 5). In order to estimate the co-ordination number of sulphur atoms in the cluster, EXAFS (extended X-ray absorption fine structure)

analysis was carried out. EXAFS for Rieske-type [2Fe-2S] cluster reflects the average co-ordination environment of the asymmetric two iron atoms in the cluster. Namely, one of the iron atoms is co-ordinated to four sulphur atoms, while the other is co-ordinated to two sulphur and two nitrogen atoms (Figure 1). The theoretical average co-ordination numbers of sulphur and nitrogen atoms are three and one respectively. Powers et al. [31] described that

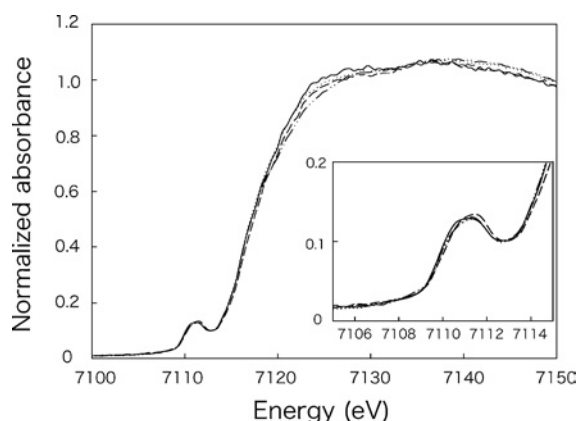


Figure 5 Iron K-edge absorption spectra of BphA3s

Normalized iron K-edge X-ray-absorption near-edge structure in the spectra of the WT protein (—), the CH mutant (···), the HC mutant (---) and the CC mutant (— · — · —). Inset, the magnified views of the pre-edge peaks. The iron concentrations of the WT protein, and the CH, HC and CC mutants were 12.2, 5.2, 4.7 and 7.5 mM respectively.

Table 2 EXAFS analysis of BphA3s

The co-ordination number of the sulphur atom (N), average Fe–S distance (r), Debye–Waller factor (σ) and R are shown. The values of N , r and σ , which were evaluated by curve-fitting analysis, are the means \pm S.E.M. R is defined as $\Sigma\{k^2\varphi_{\text{obs}}(k) - k^2\varphi_{\text{calc}}(k)\}^2 / \Sigma\{k^2\varphi_{\text{obs}}(k)\}^2$.

Protein		N	r (Å)	σ (Å ²)	R
WT	Fe–S	2.47 ± 1.43	2.25 ± 0.03	0.047 ± 0.114	0.904
	Fe–Fe	1*	2.64 ± 0.28	0.107 ± 0.153	
CH mutant	Fe–S	3.40 ± 1.34	2.30 ± 0.03	0.075 ± 0.066	0.942
	Fe–Fe	1*	2.81 ± 0.26	0.100 ± 0.133	
HC mutant	Fe–S	3.47 ± 1.32	2.26 ± 0.03	0.077 ± 0.065	0.059
	Fe–Fe	1*	2.81 ± 0.26	0.100 ± 0.133	
CC mutant	Fe–S	4.51 ± 2.87	2.30 ± 0.05	0.103 ± 0.078	0.942
	Fe–Fe	1*	2.71 ± 0.58	0.139 ± 0.291	

* Fixed parameter for the curve-fitting procedure.

standard analysis could not determine the accurate co-ordination number of nitrogen ligands per [2Fe–2S] cluster. The contribution of the Fe–N bond to the FT (Fourier transform) spectrum is smaller than that of the Fe–S bond [17]. Therefore curve-fitting analysis for first- and second-shell FT peaks was performed with the assumption that four sulphur atoms and one distant iron atom were the scattering atoms. It is noted that no Fe–N bond was considered in this assumption. Based on the crystal structure of BphF [19], the initial average Fe–S and Fe–Fe distances were set to be 2.3 and 2.7 Å respectively. The mean distance, the Debye–Waller factor and the co-ordination numbers of the sulphur atom were left as free parameters. The co-ordination number of the iron atom was fixed at 1.

The Fe–S distances in all the proteins, which were estimated by curve-fitting analysis, were approx. 2.3 Å. The evaluated co-ordination number of sulphur atoms increased with the increase in the number of histidine ligands substituted with cysteine residues (Table 2). Since the pre-edge analysis confirmed that the iron has the four-co-ordinated geometry in all the proteins, this result means that each of the iron atoms in the WT protein, in the CH and HC mutants, and in the CC mutants were co-ordinated by approx. 2.5 sulphur and 1.5 nitrogen atoms, 3.5 sulphur and 0.5 nitrogen atoms, and four sulphur atoms respectively. The average co-ordination numbers of sulphur and nitrogen atoms in the WT protein were not properly in accord with the theoretical numbers as

described above, i.e. three sulphur and one nitrogen atoms per iron atom. This discrepancy may be attributed to the absence of Fe–N contribution to the curve-fitting and/or partial degradation of the iron–sulphur cluster. Nevertheless, the increase in the co-ordination number of sulphur atoms was substantial. Moreover, the one distant iron was found to be at approx. 2.7 Å in all of these proteins. This characteristic Fe–Fe distance indicates that all the proteins contain a typical [2Fe–2S] cluster.

These edge features and the results of the EXAFS analysis probably indicates the existences of the [2Fe–2S] clusters co-ordinated by one histidine and three cysteine ligands in the CH and HC mutants, and the existence of the [2Fe–2S] cluster co-ordinated by four cysteine ligands in the CC mutant.

BphA4-dependent cytochrome *c* reduction

The cytochrome *c* reductase activities of the WT and the mutant proteins in the presence of BphA4 were analysed. All of the mutant BphA3s showed BphA4-dependent cytochrome *c* reductase activity. However, the BphA4-dependent cytochrome *c* reduction rates (k) of the mutant proteins were very low and approx. 0.1–0.3 % of that of the WT protein (Table 1), suggesting that the histidine ligands in the Rieske-type [2Fe–2S] cluster in BphA3 are critical for the electron transfer from reduced BphA4 to cytochrome *c* via BphA3.

Spectral changes caused by reduction

Spectral changes of the WT and the mutant proteins caused by the addition of sodium dithionite and by the addition of NADH in the presence of BphA4 were analysed under aerobic conditions (Figure 6). After the addition of an excess amount of sodium dithionite, the absorption spectrum of the oxidized WT BphA3 was immediately changed to a spectrum that had peaks at 432 and 510 nm (Figure 6A, a). The shape of the spectrum was characteristic of reduced Rieske-type ferredoxins [9,13,18,26]. The spectrum of the reduced WT protein returned to that of the oxidized one after autoxidation, indicating that the Rieske-type [2Fe–2S] cluster in the WT protein is reduced reversibly by sodium dithionite. The spectra of the CH and HC mutants were also rapidly changed by the addition of sodium dithionite (Figure 6A, b and c). The spectra of the CH and HC mutants just after the addition of sodium dithionite showed a shoulder at 420 nm and a peak at 530 nm, and a broad peak at 432 nm with a shoulder at approx. 520 nm respectively. Over time, the intensities of the spectra were irreversibly decreased while maintaining the same spectral shapes. In the case of the CC mutant, the intensity of the spectrum at 400–700 nm was slowly and irreversibly decreased to a very similar spectral shape (Figure 6A, d).

Spectral changes of the WT and the mutant proteins caused by the addition of NADH in the presence of BphA4, are shown in Figure 6(B). The spectrum of the WT protein was rapidly changed to a spectrum that is almost identical with that obtained by reversible reduction with dithionite (Figure 6B, a). In contrast, the intensities of the spectra of the mutants were slowly decreased without a significant spectral shape-change after the addition of NADH (Figure 6B, b–d). These spectral changes of the mutants were irreversible, suggesting that the reduced forms of the iron–sulphur cluster in the mutant proteins were unstable and rapidly destroyed.

Redox potential

The redox potentials of the WT and the mutant proteins were analysed by cyclic voltammetry. An obvious pair of anodic and

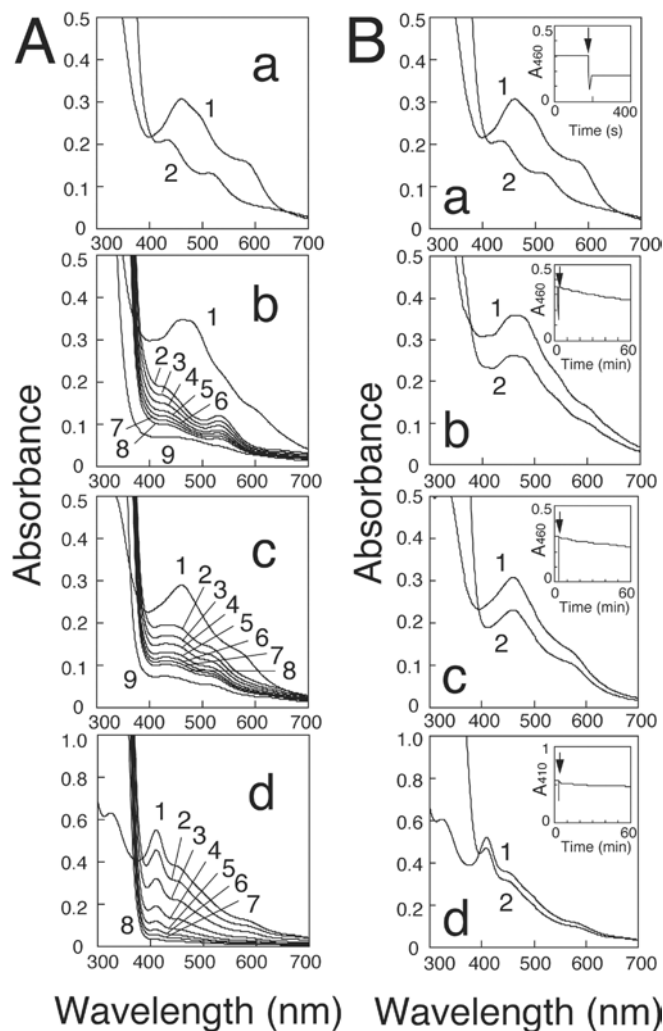


Figure 6 Spectral changes of BphA3s

(A) Spectral changes caused by the addition of excess sodium dithionite. a, The spectra of the oxidized WT protein before (1) and just after (2) the addition of sodium dithionite. b, The spectrum of the oxidized CH mutant (1), and those just after, and 10, 20, 30, 40, 50, 60 and 150 min after the addition of sodium dithionite (2–9 respectively). c, The spectrum of the oxidized HC mutant (1), and those just after, and 10, 20, 30, 40, 50, 60 and 120 min after the addition of excess sodium dithionite (2–9 respectively). d, The spectrum of the oxidized CC mutant (1) and those just after, and 5, 10, 20, 30, 40 and 60 min after the addition of sodium dithionite (lines 2–8 respectively). (B) Spectral changes caused by the addition of 300 μ M NADH in the presence of 300 nM BphA4. a, The spectrum of the oxidized WT protein (1) and that at 5 min after the addition of NADH (2). b, The spectrum of the oxidized CH mutant (1) and that at 60 min after the addition of NADH (2). c, The spectrum of the oxidized HC mutant (1) and that at 60 min after the addition of NADH (2). d, The spectrum of the oxidized CC mutant (1) and that at 60 min after the addition of NADH (2). Insets in a–d are time courses of the absorbance at 460, 460, 460 and 410 nm respectively. NADH was added at the time indicated by the arrows. In both (A) and (B), the iron concentration in the protein solution was 100 μ M.

cathodic peaks was observed in the cyclic voltammograms of the WT protein and the CH mutant, but was not observed in that of the HC and CC mutants (results not shown). In the cyclic voltammogram of the WT protein, the separation between the anodic and cathodic peak currents was 66 mV at a scan rate of 50 mV/s. The midpoint reduction potential of the WT protein was -180 ± 5 mV compared with the SHE, indicating that the WT protein is a low-potential Rieske-type ferredoxin. The CH mutant showed one reversible reduction wave at a midpoint reduction potential of

approx. -355 mV with a separation of 53 mV at the scan rate of 5 mV/s, indicating that the mutation of His⁴⁴ with a cysteine residue lowered the reduction potential of the cluster by 175 mV.

DISCUSSION

In the present study, we constructed a high-level expression system for BphA3 from *Pseudomonas* sp. KKS102 strain in *E. coli* cells, and successfully purified the WT protein by using buffer solutions containing glycerol. This expression and purification system enabled us to prepare a sufficient amount of the WT protein for structural and functional studies of the electron-transfer mechanism between BphA4 and BphA3 based on their tertiary structures. Crystallization of the WT BphA3 is in progress.

The replacement of the two histidine ligands in BphA3 with cysteine residues is tolerated for the high-level production of the mutant proteins, but the replacement with serine, asparagine and tyrosine residues is not. The amount of heterologous protein produced in *E. coli* cells is dependent on a number of factors at the transcriptional and translational levels, and on the stability of the synthesized protein. In the expression of the solubilized domain genes of porcine liver NADPH-cytochrome P450 reductase and Psb5R using pCW_{ori}⁺, which has two strong tandem *tac* promoters, the production levels of the proteins are disturbed by the intramolecular local secondary structure of mRNA, which is formed between the RBS (ribosome-binding site) and the nucleotides encoding the N-terminal region of the protein [32]. In the case of the expression plasmids for all the mutant BphA3s, the plasmid content in the cells was similar to that for the WT protein, and the mutated sites were approx. 140 and 200 bases downstream of the initiation codons and far from the RBS. In addition, *E. coli* ribonuclease E-specific AU-rich nucleotide sequence [33,34], which is specific for the mutant genes, was not found by secondary-structure prediction using the program GeneBee [35] (results not shown). Therefore we concluded that the differences in the production levels of the BphA3 mutants are not due to differences at the transcriptional level nor translational level, but at the accumulation level of the synthesized proteins. The mutant proteins, which did not accumulate to any extent in the cells, were probably unstable and degraded in the *E. coli* cells.

The X-ray absorption spectra were suggestive of the existence of [2Fe-2S] clusters, with one histidine and three cysteine ligands in the CH and HC mutants, and a [2Fe-2S] cluster, with four cysteine ligands in the CC mutant. In the crystal structure of BphF, Cys⁷, Cys⁷¹ and Cys⁸³, which are non-ligand cysteine residues conserved in BphA3, were not positioned on the cluster-binding loops [19]. The sulphur atoms of these cysteine residues were at least 10 Å away from the iron atom in the cluster co-ordinated by the histidine ligands, and seem unlikely to co-ordinate to the iron atom without a marked structural change. From these observations, it is considered that the newly introduced Cys⁴⁴ and Cys⁶⁵ in the mutants co-ordinate to the iron atom. Davidson et al. [36] replaced the histidine ligands in the Rieske protein of the ubiquinol-cytochrome *c* oxidoreductase (*bc*₁ complex) from *Rhodobacter capsulatus* with leucine, proline, phenylalanine, threonine and tyrosine, but the accumulation levels of the mutant proteins in the *E. coli* cells were very low. The substitution of a cysteine residue for His⁶⁴ in ARF, which corresponds to His⁶⁵ in BphA3, resulted in the production of a stable mutant protein, but the mutation of His⁴⁴, which corresponds to His⁴⁴ in BphA3, to a cysteine residue caused a serious destabilization of the protein [17]. In the present study, we have obtained mutant BphA3s in which His⁴⁴ and/or His⁶⁵ were replaced with cysteine residues.

To our knowledge, this is the first report of the preparation of active mutant ferredoxins, in which both of the histidine ligands of the Rieske-type [2Fe-2S] cluster are replaced with cysteine residues.

The reduction potential of the CH mutant was approx. -355 mV compared with the SHE and 175 mV lower than that of the WT BphA3, indicating that by the mutation of only one histidine ligand in BphA3 to cysteine, the reduction potential can be lowered to the level of plant-type ferredoxin (-250 to -450 mV compared with the SHE [13]). The substitution of a cysteine residue for His⁶⁴ in ARF lowered the reduction potential by at least 300 mV [17]. These results indicate that the effect of the replacement of a histidine ligand with a cysteine residue in low potential Rieske-type ferredoxin is significant. The reduction potential of the WT protein (-180 ± 5 mV compared with the SHE) was higher than that of NADH (-315 mV compared with the SHE [37]), but that of the CH mutant was lower than that of NADH. Since BphA4 rapidly reduced the wild-type BphA3 in the presence of NADH (Figure 6B, a), the midpoint reduction potential of BphA4 is probably between those of NADH and the WT protein. These potentials indicate that BphA4 cannot thermodynamically reduce the CH mutant with electrons from NADH. The slow reduction of the CH mutant by the addition of NADH in the presence of BphA4 (Figure 6B, b) and the BphA4-dependent cytochrome *c* reduction of the CH mutant are possibly due to the coupling of the reduction of oxygen in the solution and cytochrome *c* ($+235$ mV compared with the SHE [37]) respectively. Further investigation is required to clarify the reason for the low electron-transfer activities of the mutants.

The reduced iron-sulphur clusters in the CH, HC and CC mutants were significantly less stable than that in the WT protein, and were destroyed irreversibly (Figure 6). The redox-dependent structural changes of the plant-type and Rieske-type [2Fe-2S] clusters were reported previously [38–40]. In the case of the BphA3 mutants, redox-dependent structural changes, which are unfavourable to maintain the co-ordination of the ligand residues in the reduced state, may occur and result in the destruction of the cluster.

It is of interest that only the plant-type [2Fe-2S] clusters, which have four cysteine ligands, and the Rieske-type [2Fe-2S] clusters, which have two cysteine and two histidine ligands, have been found in the natural [2Fe-2S] ferredoxins, but no 'hybrid-type' [2Fe-2S] ferredoxin, with three cysteine and one histidine ligand, has been found in Nature. The instabilities of the reduced BphA3 mutants described in the present study suggest that the stability of the reduced iron-sulphur cluster is one of the important factors that determines the co-ordination patterns of amino acid residues to [2Fe-2S] clusters, in addition to the modulation of the redox potential of the cluster. Based on the results of the cysteine ligand mutations of the plant-type [2Fe-2S] cluster in the *Anabaena* 7120 vegetative ferredoxin with serine residue, Cheng et al. [28] described that Nature uses cysteine exclusively in preference to serine as the ligand of the plant-type [2Fe-2S] cluster, apparently on account of the higher stability of the complex.

We thank Dr Yasuhiro Kashino for the atomic absorption analysis, Dr Sadao Wakabayashi for amino acid sequence analysis and MS, Dr Hajime Tanida in JASRI/Spring-8 for the experimental support in the measurement of X-ray absorption spectra, Mr Noboru Kashiwagi and Mr Hirofumi Takamatsu for the preparation of recombinant BphA3 and BphA4, Dr Akio Ichimura in Osaka City University for the help with electrochemical measurements, and Dr Yasuhiro Takahashi at Osaka University, Dr Takashi Iyanagi, Dr Yoshikazu Emi, Dr Shin-ichi Ikushiro and Dr Hiroyuki Koike for helpful suggestions and discussions. This work was supported, in part, by Grants-in-Aid for Scientific Research, and by COE 21 program from the Ministry of Education, Culture, Sports, Science and Technology of Japan.

REFERENCES

- Kimbara, K., Hashimoto, T., Fukuda, M., Koana, T., Takagi, M., Oishi, M. and Yano, K. (1989) Cloning and sequencing of two tandem genes involved in degradation of 2,3-dihydroxybiphenyl to benzoic acid in the polychlorinated biphenyl-degrading soil bacterium *Pseudomonas* sp. strain KKS102. *J. Bacteriol.* **171**, 2740–2747.
- Mason, J. R. and Cammack, R. (1992) The electron-transport proteins of hydroxylating bacterial dioxygenases. *Annu. Rev. Microbiol.* **46**, 277–305.
- Kikuchi, Y., Nagata, Y., Hinata, M., Kimbara, K., Fukuda, M., Yano, K. and Takagi, M. (1994) Identification of the *bphA4* gene encoding ferredoxin reductase involved in biphenyl and polychlorinated biphenyl degradation in *Pseudomonas* sp. strain KKS102. *J. Bacteriol.* **176**, 1689–1694.
- Kikuchi, Y., Yasukochi, Y., Nagata, Y., Fukuda, M. and Takagi, M. (1994) Nucleotide sequence and functional analysis of the meta-cleavage pathway involved in biphenyl and polychlorinated biphenyl degradation in *Pseudomonas* sp. strain KKS102. *J. Bacteriol.* **176**, 4269–4276.
- Fukuda, M., Yasukochi, Y., Kikuchi, Y., Nagata, Y., Kimbara, K., Horiuchi, H., Takagi, M. and Yano, K. (1994) Identification of the *bphA* and *bphB* genes of *Pseudomonas* sp. strains KKS102 involved in degradation of biphenyl and polychlorinated biphenyls. *Biochem. Biophys. Res. Commun.* **202**, 850–856.
- Yamada, T., Sakurai, N., Nishizaki, T., Senda, T., Masai, E., Fukuda, M. and Mitsui, Y. (2000) Purification and crystallization of ferredoxin reductase component of a biphenyl dioxygenase derived from *Pseudomonas* sp. strain KKS102. *Protein Pept. Lett.* **7**, 277–280.
- Senda, T., Yamada, T., Sakurai, N., Kubota, M., Nishizaki, T., Masai, E., Fukuda, M. and Mitsui, Y. (2000) Crystal structure of NADH-dependent ferredoxin reductase component in biphenyl dioxygenase. *J. Mol. Biol.* **304**, 397–410.
- Beinert, H., Holm, R. H. and Munck, E. (1997) Iron-sulfur clusters: nature's modular, multipurpose structures. *Science* **277**, 653–659.
- Fee, J. A., Findling, K. L., Yoshida, T., Hille, R., Tarr, G. E., Hearshen, D. O., Dunham, W. R., Day, E. P., Kent, T. A. and Munck, E. (1984) Purification and characterization of the Rieske iron-sulfur protein from *Thermus thermophilus*: evidence for a [2Fe-2S] cluster having non-cysteine ligands. *J. Biol. Chem.* **259**, 124–133.
- Cline, J. F., Hoffman, B. M., Mims, W. B., LaHaie, E., Ballou, D. P. and Fee, J. A. (1985) Purification and characterization of the Rieske iron-sulfur protein from *Thermus thermophilus*. *J. Biol. Chem.* **260**, 3251–3254.
- Gurbel, R. J., Batie, C. J., Sivaraja, M., True, A. E., Fee, J. A., Hoffman, B. M. and Ballou, D. P. (1989) Electron-nuclear double resonance spectroscopy of ¹⁵N-enriched phthalate dioxygenase from *Pseudomonas cepacia* proves that two histidines are coordinated to the [2Fe-2S] Rieske-type clusters. *Biochemistry* **28**, 4861–4871.
- Shergill, J. K., Joannou, C. L., Mason, J. R. and Cammack, R. (1995) Coordination of the Rieske-type [2Fe-2S] cluster of the terminal iron-sulfur protein of *Pseudomonas putida* benzene 1,2-dioxygenase, studied by one- and two-dimensional electron spin-echo envelope modulation spectroscopy. *Biochemistry* **34**, 16533–16542.
- Couture, M. M.-J., Colbert, C. L., Babini, E., Rosell, F. I., Mauk, A. G., Bolin, J. T. and Eltis, L. D. (2001) Characterization of BphF, a Rieske-type ferredoxin with a low reduction potential. *Biochemistry* **40**, 84–92.
- Denke, E., Merbitz-Zahradnik, T., Hatzfeld, O. M., Snyder, C. H., Link, T. A. and Trumpower, B. L. (1998) Alteration of the midpoint potential and catalytic activity of the Rieske iron-sulfur protein by changes of amino acids forming hydrogen bonds to the iron-sulfur cluster. *J. Biol. Chem.* **273**, 9085–9093.
- Schroter, T., Hatzfeld, O. M., Gemeinhardt, S., Korn, M., Friedrich, T., Ludwig, B. and Link, T. A. (1998) Mutational analysis of residues forming hydrogen bonds in the Rieske [2Fe-2S] cluster of the cytochrome *bc*₁ complex in *Paracoccus denitrificans*. *Eur. J. Biochem.* **255**, 100–106.
- Guergova-Kuras, M., Kuras, R., Ugulava, N., Hadad, I. and Crofts, A. R. (2000) Specific mutagenesis of the Rieske iron-sulfur protein in *Rhodobacter sphaeroides* shows that both the thermodynamic gradient and the pK of the oxidized form determine the rate of quinol oxidation by the *bc*₁ complex. *Biochemistry* **39**, 7436–7444.
- Kounosu, A., Li, Z., Cosper, N. J., Sokes, J. E., Scott, R. A., Iai, T., Urushiyama, A. and Iwasaki, T. (2004) Engineering a three-cysteine, one-histidine ligand environment into a new hyperthermophilic archaeal Rieske-type [2Fe-2S] ferredoxin from *Sulfolobus solfataricus*. *J. Biol. Chem.* **279**, 12519–12528.
- Couture, M. M.-J., Colbert, C. L., Babini, E., Rosell, F. I., Mauk, A. G., Bolin, J. T. and Eltis, L. D. (2001) Characterization of BphF, a Rieske-type ferredoxin with a low reduction potential. *Biochemistry* **40**, 84–92.
- Colbert, C. L., Couture, M. M.-J., Eltis, L. D. and Bolin, J. T. (2000) A cluster exposed: structure of the Rieske ferredoxin from biphenyl dioxygenase and the redox properties of Rieske Fe-S proteins. *Structure* **8**, 1267–1278.

- 20 Gegner, J. A. and Dahlquist, F. W. (1991) Signal transduction in bacteria: CheW forms a reversible complex with the protein kinase CheA. *Proc. Natl. Acad. Sci. U.S.A.* **88**, 750–754
- 21 Schagger, H. and von Jagow, G. (1987) Tricine-sodium dodecyl sulfate-polyacrylamide gel electrophoresis for the separation of proteins in the range from 1 to 100 kDa. *Anal. Biochem.* **166**, 368–379
- 22 Tanida, H., Kikuchi, A., Miura, K., Takeshita, K., Goto, S., Shiro, Y. and Ishikawa, T. (2004) XAFS and protein crystallography Beamline BL38B1 at SPring-8. SRI2003 proceedings, AIP Conference Proceedings **705**, 486–489
- 23 Ankudinov, A. L., Ravel, B., Rehr, J. J. and Conradson, S. D. (1998) Real-space multiple-scattering calculation and interpretation of X-ray-absorption near-edge structure. *Phys. Rev. B Condens. Matter Mater. Phys.* **58**, 7565–7576
- 24 Kimura, T. and Suzuki, K. (1967) Component of the electron transport system in adrenal steroid hydroxylase: isolation and properties of non-heme iron protein (adrenodoxin). *J. Biol. Chem.* **242**, 485–491
- 25 Kimura, S., Emi, Y., Ikushiro, S. and Iyanagi, T. (1999) Systematic mutations of highly conserved His⁴⁹ and carboxyl-terminal of recombinant porcine liver NADH-cytochrome *b₅* reductase solubilized domain. *Biochim. Biophys. Acta* **1430**, 290–321
- 26 Link, T. A., Hatzfeld, O. M., Unalkat, P., Shergill, J. K., Cammack, R. and Mason, J. R. (1996) Comparison of the ‘‘Rieske’’ [2Fe-2S] center in the *bc₁* complex and in bacterial dioxygenases by circular dichroism spectroscopy and cyclic voltammetry. *Biochemistry* **35**, 7546–7552
- 27 Palmer, G., Brintzinger, H. and Estabrook, R. W. (1967) Spectroscopic studies on spinach ferredoxin and adrenodoxin. *Biochemistry* **6**, 1658–1664
- 28 Cheng, H., Xia, B., Reed, G. H. and Markley, J. L. (1994) Optical, EPR, and ¹H NMR spectroscopy of serine-ligated [2Fe-2S] ferredoxins produced by site-directed mutagenesis of cysteine residues in recombinant *Anabaena* 7120 vegetative ferredoxin. *Biochemistry* **33**, 3155–3164
- 29 Roe, A. L., Schneider, D. J., Mayer, R. J., Pyrz, J. W., Widom, J. and Que, Jr, L. (1984) X-ray absorption spectroscopy of iron-tyrosinate proteins. *J. Am. Chem. Soc.* **106**, 1676–1681
- 30 Colpas, G. J., Maroney, M. J., Bagyinka, C., Kumar, M., Willis, W. S., Suib, S. L., Mascharak, P. K. and Baidya, N. (1991) X-ray spectroscopic studies of nickel complexes, with application to the structure of nickel sites in hydrogenases. *Inorg. Chem.* **30**, 920–928
- 31 Powers, L., Schagger, H., von Jagow, G., Smith, J., Chance, B. and Ohnishi, T. (1989) EXAFS studies of the isolated bovine heart Rieske [2Fe-2S]^{1+(1+.2+)} cluster. *Biochim. Biophys. Acta* **975**, 293–298
- 32 Kimura, S. and Iyanagi, T. (2003) High-level expression of porcine liver cytochrome P-450 reductase catalytic domain in *Escherichia coli* by modulating the predicted local secondary structure of mRNA. *J. Biochem. (Tokyo)* **134**, 403–413
- 33 Tomcsanyi, T. and Apirion, D. (1985) Processing enzyme ribonuclease E specifically cleaves RNA I: an inhibitor of primer formation in plasmid DNA synthesis. *J. Mol. Biol.* **185**, 713–720
- 34 Liang, S.-T., Ehrenberg, M., Dennis, P. and Bremer, H. (1999) Decay of *rpIN* and *lacZ* mRNA in *Escherichia coli*. *J. Mol. Biol.* **288**, 521–538
- 35 Brodsky, L. I., Ivanov, V. V., Kalaydzidis Ya, L., Leontovich, A. M., Nikolaev, V. K., Feranchuk, S. I. and Drachev, V. A. (1995) GeneBee-NET: Internet-based server for analyzing biopolymers structure. *Biochemistry (Moscow)* **60**, 923–928
- 36 Davidson, E., Ohnishi, T., Atta-Asafo-Adjei, E. and Daldal, F. (1992) Potential ligands to the [2Fe-2S] Rieske cluster of the cytochrome *bc₁* complex of *Rhodobacter capsulatus* proved by site-directed mutagenesis. *Biochemistry* **31**, 3342–3351
- 37 Voet, D. and Voet, J. G. (2004) Oxidation–reduction reaction. In *Biochemistry* (Third edition), pp. 571–574, John Wiley & Sons, Hoboken
- 38 Cosper, N. J., Eby, D. M., Kounosu, A., Kurosawa, N., Neidle, E. L., Kurtz, Jr, D. M., Iwaski, T. and Scott, R. A. (2002) Redox-dependent structural changes in archaeal and bacterial Rieske-type [2Fe-2S] clusters. *Protein Sci.* **11**, 2969–2973
- 39 Xia, B., Volkman, B. F. and Markley, J. L. (1998) Evidence for oxidation-state-dependent conformational changes in human ferredoxin from multinuclear multidimensional NMR spectroscopy. *Biochemistry* **37**, 3965–3973
- 40 Morales, R., Charon, M.-H., Hudry-Clergeon, G., Peillot, Y., Norager, S., Medina, M. and Frey, M. (1999) Refined X-ray structures of the oxidized, at 1.3 , and reduced, at 1.17 , [2Fe-2S] ferredoxin from the cyanobacterium *Anabaena* PCC119 show redox-linked conformational changes. *Biochemistry* **38**, 15764–15773

Received 15 December 2004/24 February 2005; accepted 25 February 2005

Published as BJ Immediate Publication 25 February 2005, DOI 10.1042/BJ20042077